Computers and Mathematics with Applications 113 (2022) 52–58

Contents lists available at ScienceDirect

Computers and Mathematics with Applications

www.elsevier.com/locate/camwa

Three-dimensional volume reconstruction from multi-slice data using a shape transformation

Hyundong Kim [a], Chaeyoung Lee [a], Soobin Kwak [a], Youngjin Hwang [a], Sangkwon Kim [a], Yongho Choi [b], Junseok Kim [a,*]

[a] Department of Mathematics, Korea University, Seoul 02841, Republic of Korea
[b] Department of Mathematics and Big Data, Daegu University, Gyeongsan-si, Gyeongsangbuk-do 38453, Republic of Korea

ARTICLE INFO

Dataset link: https://doi.org/10.24433/CO.8740802.v1

Keywords:
Volume reconstruction
Finite difference method
Shape transformation
Phase-field model

ABSTRACT

We present a computational method for the 3D volume reconstruction from cross-sectional data. The proposed method is based on the Allen–Cahn (AC) equation with a source term. The source term is related to shape transformation from a source object to a target object. Using the operator splitting method, the governing equation is solved by splitting it into three steps. The numerical solution is obtained explicitly using the Euler's methods and the separation of variables. To reconstruct the 3D object from two slice data, we set one slice as the target data and the other data as the initial data. We solve the governing equation and stack intermediate solutions based on the relative fraction of the symmetric difference of two regions occupied by the target and source data. To demonstrate that the proposed method can reconstruct a 3D model through extracted intermediate slice data during shape transformation, we perform several computational tests. Furthermore, the proposed method is applied to a 3D volume reconstruction from multi-slice data of human vertebra.

1. Introduction

Advances in imaging techniques such as a computed tomography (CT) have accelerated the visualizing slice data or internal anatomy. It is possible to accurately analyze brain bleeding, organ bleeding, and complex fractures, etc., which are caused by accidents in which a large physical force is applied from the outside such as traffic accidents and fall accidents and then carry on treatment. The reason why fast and accurate analysis and treatment was possible is because the diagnosis was performed by applying volumetric reconstruction based on appropriate adjacent slices without dividing and analyzing hundreds of comprised large volumes of complex clinical database slices. The three-dimensional geometrical models created by applying volume reconstruction under computer aid undoubtedly helped surgeons improve their diagnosis. For this reason, we research a 3D volume reconstruction of multi-slice data using shape transformation in this study.

Studies to reconstruct the three-dimensional shape by using slice data have been researched in a variety of methods. In earlier studies, fast reconstruction technique by reducing the problem which constructing a sequence of partial approximations when connecting two contour lines in adjacent planes was studied [1]. The computer-aided anatomical reconstruction system was developed, and the system provides calculating the volumes, lengths and surface areas [2]. To reconstruct a smooth 3D object from serial cross sections, a robust algorithm was proposed in [3]. The univariate contour interpolation method was used along with the approximate gradient directions of the unknown surface to solve bivariate problems [4]. They suggested C^1-continuous terrain reconstruction, however, the other research [5] considered the reconstructed surface to be at least C^2-continuous. To reconstruct the consistent d-dimensional surface from $(d-1)$-dimensional slices under some constraints, phase-field models were proposed [6]. The partial differential equation model was presented in [7], which has a penalization term and parameter control term for 3D smooth surfaces reconstruction from 2D parallel slices. The helical filtered back-projection, compressed sensing, and more recent deep learning techniques were considered for accurate volume reconstruction by improving the problems of multi-row detector CT scanners [8]. An adaptive reconstruction method was presented in [9] that processes MRI images of fetal brains damaged

The code (and data) in this article has been certified as Reproducible by Code Ocean: https://codeocean.com/. More information on the Reproducibility Badge Initiative is available at https://www.elsevier.com/physical-sciences-and-engineering/computer-science/journals.

* Corresponding author.
E-mail addresses: rlagusehd@korea.ac.kr (H. Kim), cfdkim@korea.ac.kr (J. Kim).
URL: https://mathematicians.korea.ac.kr/cfdkim/ (J. Kim).

https://doi.org/10.1016/j.camwa.2022.03.018
Received 18 June 2021; Received in revised form 10 January 2022; Accepted 6 March 2022

by artifacts and reconstruct volume using sliced images. Images with 80–90% data removed were also reconstructed as super-resolution images. In recent years, not only studies on 3D volume reconstruction from slice data using numerical methods, but also studies on 3D volume reconstruction from slices using convolutional neural network techniques have been conducted [10,11].

The phase-field models have been frequently applied for volume reconstruction [12–16] and repairing [17]. Using image segmentation method based on the modified Cahn–Hilliard equation with a fidelity term [18], the initial slice data obtained from given CT or MRI images, multi objects can be constructed. This proposed method was extended from binary system to multi-component system [19]. Furthermore, the proposed method introduced in [18] was improved by adding a preprocessing step for smoothing the slice constraints [20].

In this study, we propose a simple and explicit computational algorithm for the volume reconstruction using extracted slice data during shape transformation. To perform the shape transformation, we use a modified Allen–Cahn (AC) equation [21]. Its numerical algorithm is obtained using the Euler's methods and closed-form solution, therefore, the numerical algorithm is constructed simply and explicitly.

The presented study consists of the following sections. We present the phase-field model and its algorithm of numerical solution in Section 2. In Section 3, we implement the numerical tests for volume reconstruction using a shape transformation. Conclusions are offered in Section 5.

2. Modified AC equation and computational solution

2.1. Modified AC equation

We propose the following phase-field model [21] for the volume reconstruction using a shape transformation.

$$\frac{\partial \phi(\mathbf{x},t)}{\partial t} = -\frac{F'(\phi(\mathbf{x},t))}{\epsilon^2} + \Delta\phi(\mathbf{x},t) + \alpha\sqrt{F(\phi(\mathbf{x},t))}(\psi(\mathbf{x}) - \phi(\mathbf{x},t)),\ \mathbf{x}\in\Omega,\ t>0, \tag{1}$$

where $\phi(\mathbf{x},t)$ is the phase-field, ϵ is a positive constant, α is a parameter that controls fidelity, and $F(\phi) = (\phi^2-1)^2/4$. We denote the source and target shapes by $\phi(\mathbf{x},0)$ and $\psi(\mathbf{x})$, respectively.

2.2. Numerical solution algorithm

In the 2D space $\Omega = (a,b)\times(c,d)$, we shall discretize Eq. (1) to find the numerical solution. Let N_x and N_y be the numbers of cells, and $h = (b-a)/N_x = (d-c)/N_y$ be the grid size. We set the discrete domain $\Omega = \{(x_i,y_j):\ x_i = a+hi,\ y_j = c+hj,\ 0\le i\le N_x,\ 0\le j\le N_y\}$. The discrete approximation of $\phi(x_i,y_j,n\Delta t)$ is denoted by ϕ_{ij}^n, where Δt is the time step size. Now, we split Eq. (1) using the operator splitting method into

$$\frac{\partial \phi(\mathbf{x},t)}{\partial t} = \Delta\phi(\mathbf{x},t), \tag{2}$$

$$\frac{\partial \phi(\mathbf{x},t)}{\partial t} = -\frac{F'(\phi(\mathbf{x},t))}{\epsilon^2}, \tag{3}$$

$$\frac{\partial \phi(\mathbf{x},t)}{\partial t} = \alpha\sqrt{F(\phi(\mathbf{x},t))}(\psi(\mathbf{x}) - \phi(\mathbf{x},t)). \tag{4}$$

Through the following three steps, we can find the numerical solution of Eq. (1). To begin with, we solve the diffusion term (2) using the explicit Euler's scheme:

$$\frac{\phi_{ij}^* - \phi_{ij}^n}{\Delta t} = \Delta_d\phi_{ij}^n, \tag{5}$$

where $\Delta_d\phi_{ij}^n = (\phi_{i+1,j}^n + \phi_{i-1,j}^n + \phi_{i,j+1}^n + \phi_{i,j-1}^n - 4\phi_{ij}^n)/h^2$ with a Dirichlet boundary condition. Equation (5) can be rewritten as $\phi_{ij}^* = \phi_{ij}^n + \Delta t\Delta_d\phi_{ij}^n$. Next, we can derive the closed-form solution of the reaction term (3) applying separation of variables:

$$\phi_{ij}^{**} = \phi_{ij}^* \Big/ \sqrt{\left(1-\left(\phi_{ij}^*\right)^2\right)e^{-\frac{2\Delta t}{\epsilon^2}} + \left(\phi_{ij}^*\right)^2}. \tag{6}$$

For more details about the explicit AC equation solver, see [22]. For solving the fidelity term (4), the implicit Euler's scheme with the frozen coefficient $\sqrt{F\left(\phi_{ij}^{**}\right)}$ is adopted:

$$\frac{\phi_{ij}^{n+1} - \phi_{ij}^{**}}{\Delta t} = \alpha\sqrt{F\left(\phi_{ij}^{**}\right)}(\psi_{ij} - \phi_{ij}^{n+1}). \tag{7}$$

Finally, we get

$$\phi_{ij}^{n+1} = \frac{\phi_{ij}^{**} + \Delta t\alpha\psi_{ij}\sqrt{F\left(\phi_{ij}^{**}\right)}}{1+\Delta t\alpha\sqrt{F\left(\phi_{ij}^{**}\right)}}. \tag{8}$$

The proposed numerical algorithm for constructing a volume from two slice data is as follows. Let $\Omega_1(t)$ and $\Omega_2(t)$ be two time-dependent domains; and $\Omega_1(0) = S_1$ and $\Omega_2(0) = S_2$ be two given slice data, see Fig. 1(a) and (b), respectively. If we set $\Omega_2(t)$ as the target data, then $\Omega_2(t) = S_2$ for all time t. We can represent $\Omega_1(t) = \{\mathbf{x}|\phi(\mathbf{x},t)\ge 0\}$ and $\Omega_2(0) = \{\mathbf{x}|\psi(\mathbf{x})\ge 0\}$ using $\phi(\mathbf{x},t)$ and $\psi(\mathbf{x})$. Fig. 1(c) shows an intermediate shape $\Omega_1(t)$ at some time $t>0$.

Let $\mathcal{A}(t) = Area\left((\Omega_1(t)\cup S_2)\setminus(\Omega_1(t)\cap S_2)\right)$ be the area of the set $(\Omega_1(t)\cup S_2)\setminus(\Omega_1(t)\cap S_2)$ at time t as shown in Fig. 1(d). During shape transformation from source data S_1 to target data S_2, we save intermediate data $\Omega_1(t)$ at time t, based on $\mathcal{A}(t)$. Here, the gradually saved intermediate data are used as cross-sectional slice data that can reconstruct the 3D volume. This stacking process schematically illustrated in Fig. 1(e) and (f).

Let N_z be an integer, which is the number of slice data that we want to have between the two given slice data. Let Ψ_{ijk} be a three-dimensional reconstructed volume data which is defined on $\Omega_V = \{(x_i,y_j,z_k):\ x_i = a+hi,\ y_j = c+hj,\ z_k = hk,\ 0\le i\le N_x,\ 0\le j\le N_y,\ 0\le k\le N_z+1\}$. We define the three-dimensional volume as

$$\Psi_{ijk} = \begin{cases} \phi_{ij}^0 & \text{if } k=0,\\ \phi_{ij}^{n_k} & \text{if } k=1,\dots,N_z,\\ \psi_{ij} & \text{if } k=N_z+1, \end{cases} \tag{9}$$

where n_k the minimum integer which satisfies the following condition

$$\mathcal{A}(n_k\Delta t) \le \frac{N_z+1-k}{N_z+1}\mathcal{A}(0), \tag{10}$$

where $\mathcal{A}(0) = \sum_{i=1}^{N_x}\sum_{j=1}^{N_y}\left|\frac{\psi_{ij}-\phi_{ij}^0}{2}\right|h^2$ is an initial area excluding the intersection of the source S_1 and target S_2. Fig. 1(g) shows the isosurface of Ψ at level zero.

3. Numerical tests

To show the performance of the proposed method for constructing the 3D volume object using slice data, we conduct the numerical experiments. The proposed method consists of the following three steps:

First, we define the 2D initial source $\phi(\mathbf{x},0)$, target $\psi(\mathbf{x})$, and the number of slices N_z.

Second, we perform transformation and save slice data which satisfies Eq. (10) for volume construction.

Third, we construct the 3D volume object from saved slice data in the second step.

Unless otherwise stated, we set the parameter values as $N_x = N_y = 150$, $\Delta t = 0.15h^2$, $\epsilon = h$ and $\alpha = 3000$ in this study. In addition, let us define the following notations for the simplicity of exposition:

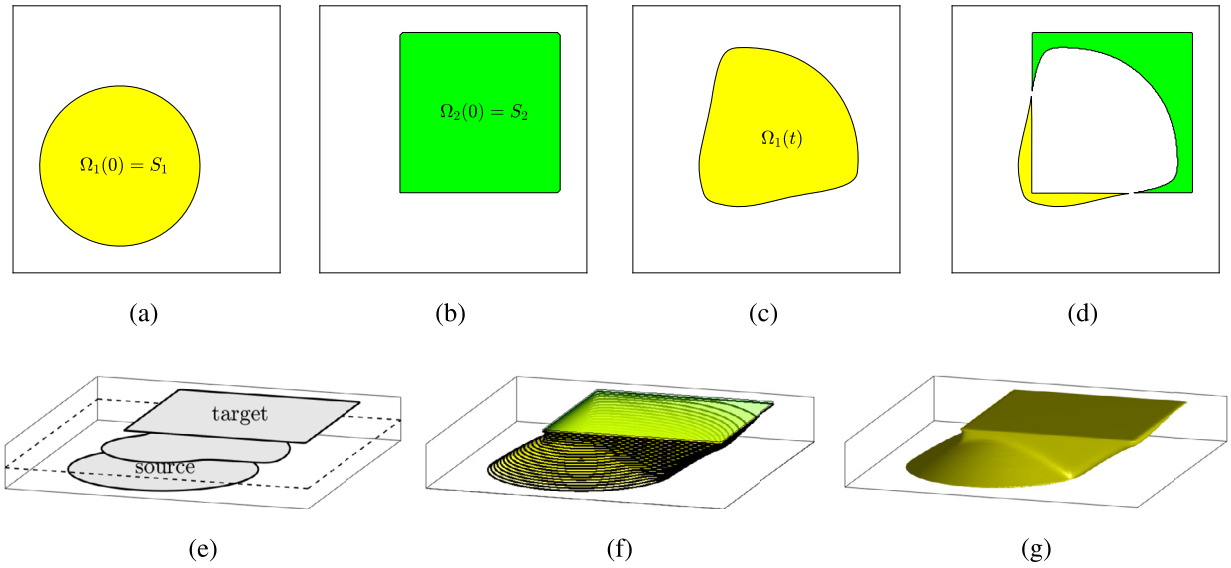

Fig. 1. Schematic illustration of (a) source shape $\Omega_1(0)$, (b) target shape S_2, (c) intermediate shape $\Omega_1(t)$ with $t > 0$, (d) $(\Omega_1(t) \cup S_2) \setminus (\Omega_1(t) \cap S_2)$ at time t, (e) source, target, and an intermediate shapes, (f) multiple stacking, and (g) isosurface of Ψ at level zero.

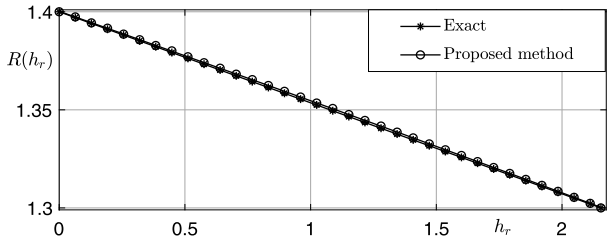

Fig. 2. Radii of the slice disks from the exact and reconstructed volumes with respect to height h_r.

$$C(x, y; x_0, y_0, r) = \tanh\left(\frac{r - \sqrt{(x-x_0)^2 + (y-y_0)^2}}{\sqrt{2}\epsilon}\right),$$

$$S(x, y; x_0, y_0, a, b) = \tanh\left(\frac{\min(a - |x - x_0|, b - |y - y_0|)}{\sqrt{2}\epsilon}\right).$$

3.1. Quantitative test

We perform a quantitative test with a larger circle source $\phi(x, y, 0)$ and a smaller circle target $\psi(x, y)$ on $\Omega = [0,\ 3.2] \times [0,\ 3.2]$:

$$\phi(x, y, 0) = C(x, y; 1.6, 1.6, 1.4) \quad \text{and} \quad \psi(x, y) = C(x, y; 1.6, 1.6, 1.3).$$

The parameters used are as follows: $N_x = N_y = 150$, $N_z = 100$, $h = 3.2/N_x$, $\Delta t = 0.005h^2$, and $\alpha = 3000$. As shown in Fig. 2, we can see that the radii of the slice disks from the exact and reconstructed volumes are in good agreement with each other.

3.2. Volume reconstruction from circle source to square target

We perform the numerical experiment for the 3D volume reconstruction using extracted slice data during shape transformation from the circle source to the square target. In Fig. 3, the source $\phi(x, y, 0)$ and target $\psi(x, y)$ on $\Omega = [0,\ 2] \times [0,\ 2]$ are given as

$$\phi(x, y, 0) = C(x, y; 0.8, 0.8, 0.6) \text{ and } \psi(x, y) = S(x, y; 1.2, 1.2, 0.6, 0.6).$$

Fig. 3(a) shows the snapshots of shape transformation from the circle source to the square target. Fig. 3(b) is the numerical result for the 3D volume reconstruction using extracted $N_z = 20$ slices data during shape transformation.

3.3. Volume reconstruction from three circles source to one circle target

We perform the volume reconstruction from the three circles source to the one circle target. We set the source $\phi(x, y, 0)$ and target $\psi(x, y)$ on the computational domain $\Omega = [0,\ 2] \times [0,\ 2]$ are given as

$$\phi(x, y, 0) = C(x, y; 1.4, 0.6, 0.2) + C(x, y; 1.4, 1.4, 0.2) + C(x, y; 0.4, 1, 0.2) + 2,$$
$$\psi(x, y) = C(x, y; 1, 1, 0.6).$$

Fig. 4(a) shows the snapshots of shape transformation from the three circles source to the one circle target. Figs. 4(b) and (c) are volume reconstruction using extracted $N_z = 20$ and $N_z = 40$ slices data during shape transformation, respectively.

3.4. Volume reconstruction from annulus source to circle target

Now, we consider the annulus source $\phi(x, y, 0)$ and circle target $\psi(x, y)$ on $\Omega = [0,\ 2] \times [0,\ 2]$ as

$$\phi(x, y, 0) = C(x, y; 1, 1, 0.8) - C(x, y; 1, 1, 0.4) - 1,$$
$$\psi(x, y) = C(x, y; 1, 1, 0.5).$$

The numerical results for the shape transformation can be seen in Fig. 5(a). As shown in Figs. 5(b) and (c), two different topologies are smoothly merged together and the 3D volumes are reconstructed.

3.5. Volume reconstruction from complex shapes

On $\Omega = [0,\ 2] \times [0,\ 2]$, the initial condition in Fig. 6(a) is set to

$$\begin{aligned}\phi(x, y, 0) = {} & C(x, y; 0.6, 0.6, 0.3) - C(x, y; 0.6, 0.6, 0.1) + C(x, y; 0.6, 1.4, 0.3) \\ & - C(x, y; 0.6, 1.4, 0.1) + C(x, y; 1.4, 0.6, 0.3) - C(x, y; 1.4, 0.6, 0.1) \\ & + C(x, y; 1.4, 1.4, 0.3) - C(x, y; 1.4, 1.4, 0.1) - 1,\end{aligned}$$

$$\begin{aligned}\psi(x, y) = {} & S(x, y; 1, 1, 0.8, 0.8) - S(x, y; 0.6, 0.6, 0.2, 0.8) \\ & - S(x, y; 0.6, 1.4, 0.2, 0.8) \\ & - S(x, y; 1.4, 0.6, 0.2, 0.8) - S(x, y; 1.4, 1.4, 0.2, 0.8) - 4.\end{aligned}$$

Here, we use the same parameter values in the previous test. In this numerical experiment, we use more complex shapes as the source and target. To obtain the well-reconstructing volume as shown in Fig. 6(b) and (c), we use a larger value of fidelity parameter.

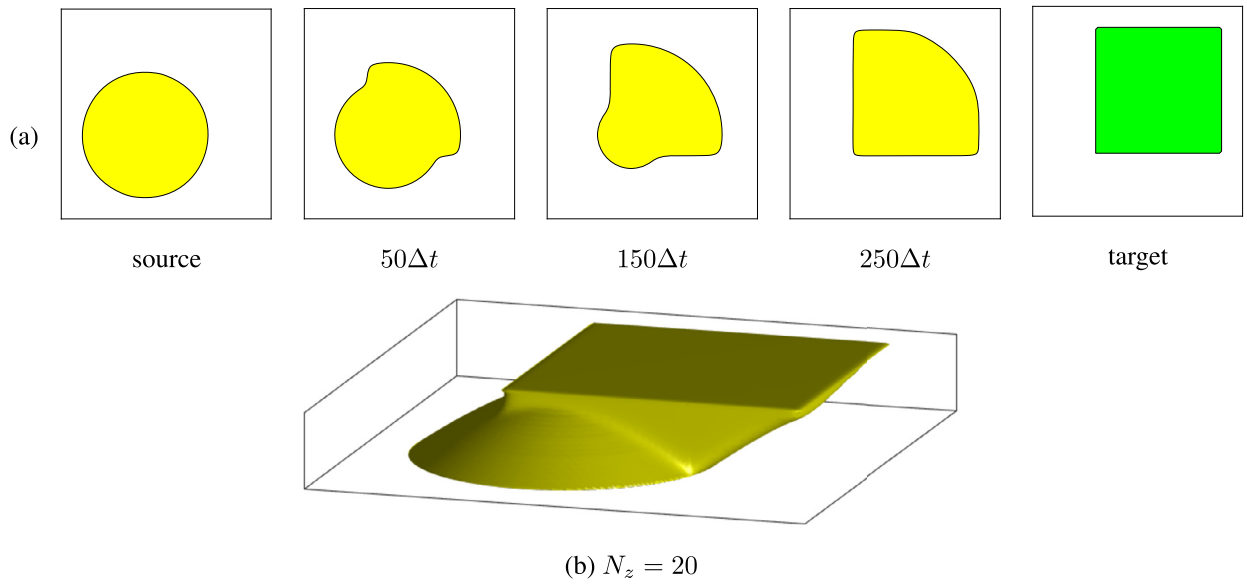

Fig. 3. Snapshots of (a) shape transformation from circle source to square target and (b) numerical result for 3D volume reconstruction using extracted 20 slices data during shape transformation.

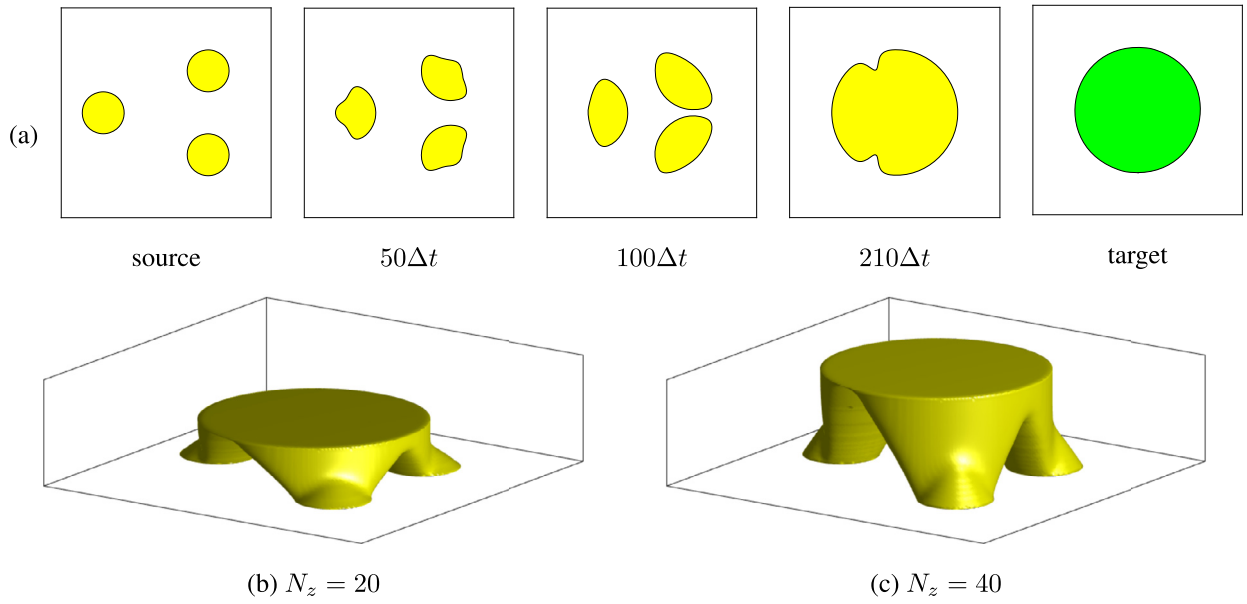

Fig. 4. Snapshots of (a) shape transformation from three circle source to one circle target. (b) and (c) numerical results for 3D volume reconstruction using extracted 20 and 40 slices data during shape transformation, respectively.

3.6. Volume reconstruction from multi slice data

Now, we perform the volume reconstruction from multi slice data, which is shown in Fig. 7. We shall use the multi slice data of human vertebra shape, shown in Fig. 8(a), which was reconstructed in a precedent research [18]. We set the domain size as $\Omega = [0,\ 1] \times [0,\ 1]$, and the parameter values as $N_x = N_y = 160$, $\Delta t = 0.001h^2$, $\epsilon = 2h$ and $\alpha = 1.0e + 06$.

First, we partition human vertebra in Fig. 8(a) into $N_z = 72$ grids along the z-axis, and then choose $(3 + 5s)$th, 69th and 72th slices, ($s = 0, \ldots, 13$). The slice data chosen for volume reconstruction can be found in Fig. 7 ordered from left to right and from top to bottom.

Second, we perform a volume reconstruction using the proposed method. The reconstructed volume is presented in Fig. 8(b). Here, comparing with the original human vertebra in Fig. 8(a), it can be seen that the reconstructed volume has non-smooth result. To make the result smooth, we conduct the post-processing by the three-dimensional heat equation with a fidelity term [23]. The smooth numerical result after post-processing can be seen in Fig. 8(c).

4. Discussions

Because real CT data sets may contain noises, image segmentation techniques are required to extract images for volume reconstruction. Therefore, to obtain slice data from real CT data sets, we can consider the following modified Allen–Cahn equation with edge-stopping function [24] for an image segmentation as a pre-processing step before reconstructing the volume:

$$\frac{\partial \phi(\mathbf{x},t)}{\partial t} = g\left(f_0(\mathbf{x})\right)\left(-\frac{F'(\phi(\mathbf{x},t))}{\epsilon^2} + \Delta\phi(\mathbf{x},t)\right) + \beta\, g\left(f_0(\mathbf{x})\right) F(\phi(\mathbf{x},t)),$$

where the detailed expressions of the parameters and functions used can be found in [24]. (See Fig. 9.)

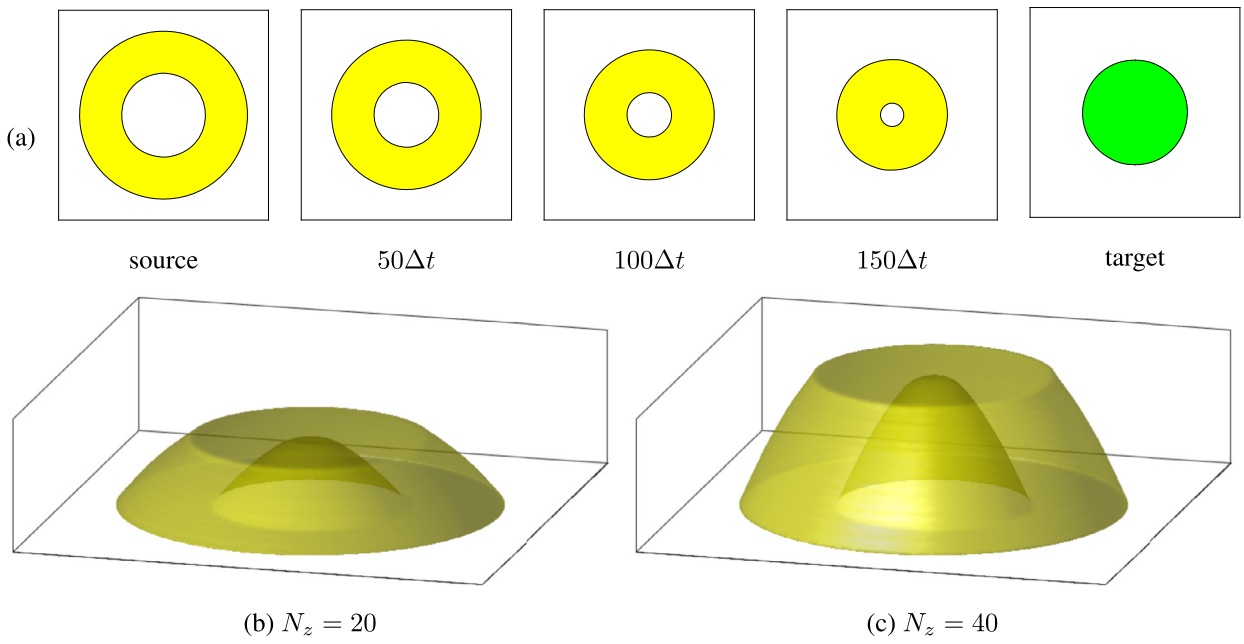

Fig. 5. Snapshots of (a) shape transformation from source to target. (b) and (c) numerical results for 3D volume reconstruction using extracted 20 and 40 slices data during shape transformation, respectively.

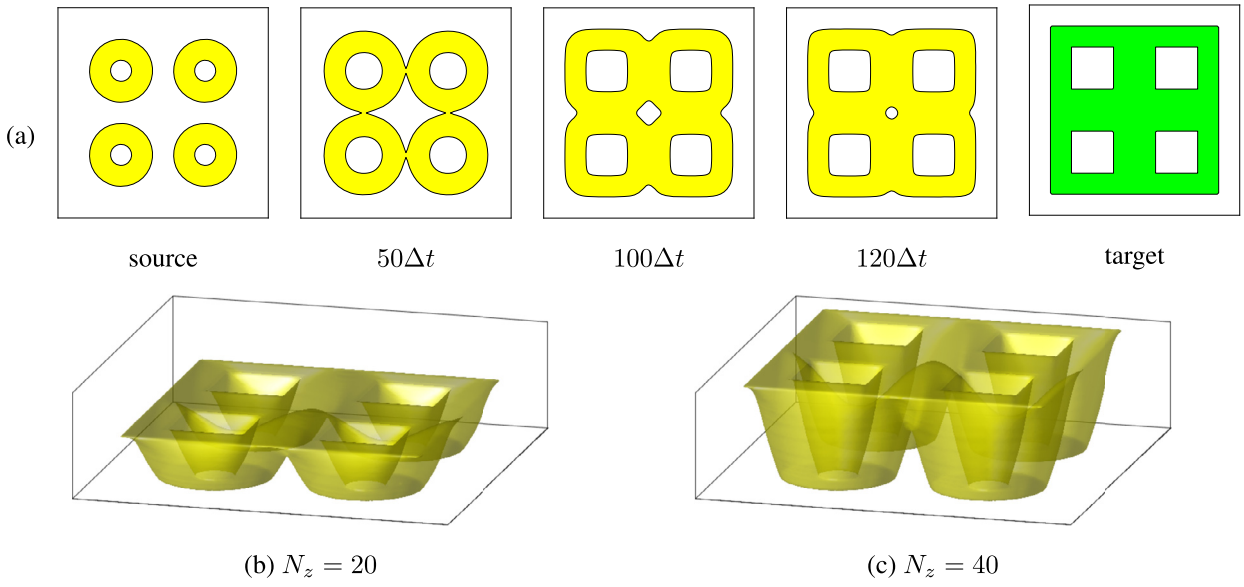

Fig. 6. Snapshots of (a) shape transformation from four annulus source to four squares target. (b) and (c) are the numerical results for 3D volume reconstruction using extracted 20 and 40 slices data during shape transformation, respectively.

Next, we investigate the CPU times of main iterations in the proposed algorithm. Here, the numerical experiments are performed on Intel Core i5-9400 CPU at 2.90 GHz with 8 GB RAM. Table 1 shows the measured total CPU time, the number of iteration steps and the average CPU time per iteration.

We compare the computational complexity between the proposed method and multigrid method. The multigrid method is an iterative method which is widely employed for solving partial differential equations implicitly, and also used in [18]. Typically, the relaxation part in the multigrid method uses the Gauss–Seidel method. We define the computational cost of one relaxation sweep as a work unit (WU) and the number of relaxation sweeps for a V-cycle as a positive integer ν larger than 1. The computational complexity of a V-cycle is less than 8ν WU/3 as induced in [25]. In [18], the authors performed the simulation in Fig. 8 with a $160 \times 160 \times 72$ mesh grid and obtained the result after 14 iterations, therefore, the computational complexity is

Table 1
Total CPU time, the number of iteration steps, average CPU time per iteration. $N_z = 40$ is used in all CPU tests.

Cases	Total CPU time (s)	Iteration steps	Average CPU time (s)
Fig. 3	3.3569e-01	322	1.0425e-03
Fig. 4	2.5576e-01	228	1.0003e-03
Fig. 5	2.1722e-01	170	1.2778e-03
Fig. 6	2.6047e-01	142	1.8343e-03
Fig. 8	5.3088e+00	634	8.4000e-03

Fig. 7. Multi slice data of human vertebra.

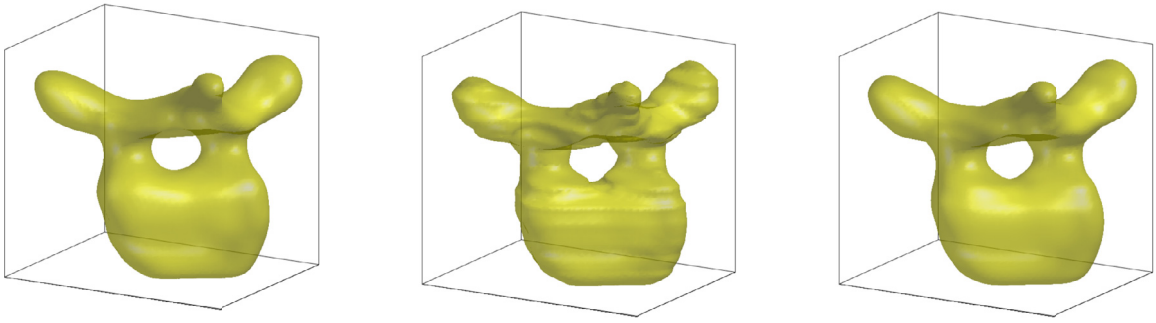

(a) Human vertebra (b) Before smoothing step (c) After smoothing step

Fig. 8. Reconstructed human vertebra from multi slice data in a precedent research [18]. (a) Human vertebra, (b) volume reconstruction using the proposed method, and (c) volume after post-processing.

$160 \times 160 \times 72 \times 14 \times 8\nu$ WU/3. On the other hand, the computational complexity of the proposed method in this study, is $160 \times 160 \times 654$ WU because we use 2D slices with a mesh grid 160×160 and reconstruct the 3D volume after 654 iterations using the proposed method. Therefore, it can be seen that the computational cost of the proposed method is reduced by at least 4ν times compared to the previous work. The advantage of the proposed method is simple and fast. It requires less computational cost compared with multigrid method.

5. Conclusions

In this study, we proposed a numerical algorithm for the 3D volume reconstruction from the multi cross-sectional data using the AC equation with a source term. The source term is related to shape transformation, which is a process of transforming from a source object to a target object. The numerical solution algorithm is based on the operator splitting method and all the steps are explicit, therefore, the

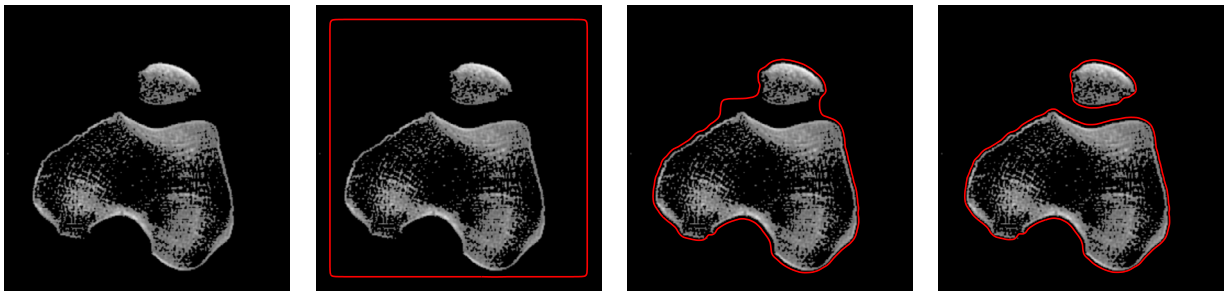

Fig. 9. Image segmentation. Reprinted from Yibao Li et al. [18] with permission from Elsevier.

scheme is simple to implement. Several numerical tests demonstrated the performance of the proposed method. The volume reconstruction was performed using the proposed method from multi-slice data of human vertebra. To have smooth result, we adopted the post-processing using the three-dimensional diffusion equation with a fidelity term.

Link to the Reproducible Capsule

https://doi.org/10.24433/CO.8740802.v1

Acknowledgement

The first author (Hyundong Kim) was supported by Basic Science Research Program through the National Research Foundation of Korea (NRF) funded by the Ministry of Education (NRF-2020R1A6A3A13077105). Chaeyoung Lee was supported by Basic Science Research Program through the National Research Foundation of Korea (NRF) funded by the Ministry of Education (NRF-2019R1A6A3A13094308). Yongho Choi was supported by the National Research Foundation of Korea (NRF) grant funded by the Korea government (NRF-2020R1C1C1A0101153712). The corresponding author (Junseok Kim) was supported by Korea University Grant. The authors are grateful to the reviewers for the constructive and helpful comments on the revision of this article.

References

[1] H. Fuchs, Z.M. Kedem, S.P. Uselton, Optimal surface reconstruction from planar contours, Commun. ACM 20 (10) (1977) 693–702.
[2] E.M. Johnson, J.J. Capowski, A system for the three-dimensional reconstruction of biological structures, Comput. Biomed. Res. 16 (1) (1983) 79–87.
[3] W.C. Lin, S.Y. Chen, C.T. Chen, A new surface interpolation technique for reconstructing 3D objects from serial cross-sections, Comput. Vis. Graph. Image Process. 48 (1) (1989) 124–143.
[4] K. Hormann, S. Spinello, P. Schröder, C1-continuous terrain reconstruction from sparse contours, in: VMV 3, 2003.
[5] S.U. Kim, C.O. Lee, Accurate surface reconstruction in 3d using two–dimensional parallel cross sections, J. Math. Imaging Vis. 53 (2) (2015) 182–195.
[6] E. Bretin, F. Dayrens, S. Masnou, Volume reconstruction from slices, SIAM J. Imaging Sci. 10 (4) (2017) 2326–2358.
[7] Q. Zou, A PDE model for smooth surface reconstruction from 2D parallel slices, IEEE Signal Process. Lett. 27 (2020) 1015–1019.
[8] J.W. Hayes, J. Montoya, A. Budde, C. Zhang, Y. Li, K. Li, J. Hsieh, G.H. Chen, High pitch helical CT reconstruction, IEEE Trans. Med. Imaging 40 (11) (2021) 3077–3088.
[9] Q. Ni, Y. Zhang, T. Wen, L. Li, A sparse volume reconstruction method for fetal brain MRI using adaptive kernel regression, BioMed Res. Int. 2021 (2021) 6685943.
[10] Z. Chen, Z. Xu, W. Yi, X. Yang, W. Hou, M. Ding, O. Granichin, Real–time and multimodal brain slice-to-volume registration using CNN, Expert Syst. Appl. 133 (2019) 86–96.
[11] Z. Chen, Z. Xu, Q. Gui, X. Yang, Q. Cheng, W. Hou, M. Ding, Self–learning based medical image representation for rigid real-time and multimodal slice-to-volume registration, Inf. Sci. 541 (2020) 502–515.
[12] Y. Li, D. Lee, C. Lee, J. Lee, S. Lee, J. Kim, S. Ahn, J. Kim, Surface embedding narrow volume reconstruction from unorganized points, Comput. Vis. Image Underst. 121 (2014) 100–107.
[13] Y. Li, J. Kim, Fast and efficient narrow volume reconstruction from scattered data, Pattern Recognit. 48 (12) (2015) 4057–4069.
[14] S. Lee, Y. Choi, D. Lee, H.K. Jo, S. Lee, S. Myung, J. Kim, A modified Cahn–Hilliard equation for 3D volume reconstruction from two planar cross sections, J. Korean Soc. Ind. Appl. Math. 19 (1) (2015) 47–56.
[15] D. Jeong, Y. Li, H.J. Lee, S.M. Lee, J. Yang, S. Park, H. Kim, Y. Choi, J. Kim, Efficient 3D volume reconstruction from a point cloud using a phase-field method, Math. Probl. Eng. 2018 (2018).
[16] J. Wang, Z. Shi, Multi-reconstruction from points cloud by using a modified vector-valued Allen—Cahn equation, Mathematics 9 (12) (2021) 1326.
[17] Y. Li, S. Lan, X. Liu, B. Lu, L. Wang, An efficient volume repairing method by using a modified Allen–Cahn equation, Pattern Recognit. 107 (2020) 107478.
[18] Y. Li, J. Shin, Y. Choi, J. Kim, Three-dimensional volume reconstruction from slice data using phase-field models, Comput. Vis. Image Underst. 137 (2015) 115–124.
[19] Y. Li, J. Wang, B. Lu, D. Jeong, J. Kim, Multicomponent volume reconstruction from slice data using a modified multicomponent Cahn–Hilliard system, Pattern Recognit. 93 (2019) 124–133.
[20] J. Kim, C.O. Lee, Three-dimensional volume reconstruction using two-dimensional parallel slices, SIAM J. Imaging Sci. 12 (1) (2019) 1–27.
[21] H. Kim, S. Yoon, J. Wang, C. Lee, S. Kim, J. Park, J. Kim, Shape transformation using the modified Allen—Cahn equation, Appl. Math. Lett. 107 (2020) 106487.
[22] D. Jeong, J. Kim, An explicit hybrid finite difference scheme for the Allen—Cahn equation, J. Comput. Appl. Math. 340 (2018) 247–255.
[23] A.L. Bertozzi, S. Esedoglu, A. Gillette, Inpainting of binary images using the Cahn—Hilliard equation, IEEE Trans. Image Process. 16 (1) (2006) 285–291.
[24] Y. Li, J. Kim, A fast and accurate numerical method for medical image segmentation, J. Korean Soc. Ind. Appl. Math. 14 (4) (2010) 201–210.
[25] J. Yang, C. Lee, S. Kwak, Y. Choi, J. Kim, A conservative and stable explicit finite difference scheme for the diffusion equation, J. Comput. Sci. 56 (2021) 101491.